
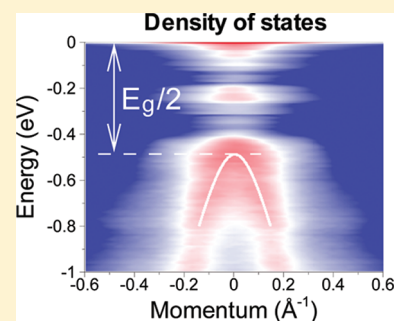


Scaling of the Energy Gap in Pattern-Hydrogenated Graphene

Roberto Grassi,^{*,†,‡} Tony Low,^{†,§} and Mark Lundstrom[†][†]School of Electrical & Computer Engineering, Purdue University, West Lafayette, Indiana 47906, United States[‡]ARCES and DEIS, University of Bologna, Viale Risorgimento 2, 40136 Bologna, Italy Supporting Information

ABSTRACT: Recent experiments show that a substantial energy gap in graphene can be induced via patterned hydrogenation on an iridium substrate. Here, we show that the energy gap is roughly proportional to $N_{\text{H}}^{1/2}/N_{\text{C}}$ when disorder is accounted for, where N_{H} and N_{C} denote concentrations of hydrogen and carbon atoms, respectively. The dispersion relation, obtained through calculation of the momentum-energy resolved density of states, is shown to agree with previous angle-resolved photoemission spectroscopy results. Simulations of electronic transport in finite size samples also reveal a similar transport gap, up to 1 eV within experimentally achievable $N_{\text{H}}^{1/2}/N_{\text{C}}$ values.

KEYWORDS: Graphene, hydrogenation, superlattice, disorder, energy gap, scaling



Graphene's novel electronic and physical properties make it an interesting material for various potential applications.^{1,2} For electronics, the absence of an energy gap limits its applicability. Currently, there are myriad known ways to opening an energy gap in graphene. For instance, the patterning of graphene nanoribbons induces a band gap due to the confinement of carriers along the transverse direction.³ Although there are recent proposals in achieving controlled width and smooth edges,⁴ the large scale fabrication of nanoribbons remains a challenge. The graphene nanomesh, also known as a graphene antidot lattice, is a viable alternative.^{5,6} Here, the confinement potential is created by clusters of vacancies, i.e., nanoholes, arranged on a regular superlattice. They are prepared using block copolymer lithography. Two structural parameters, the cluster size and neck width of the superlattice of nanoholes, govern the electronic transport properties observed in experiments.⁶ A larger energy gap is induced when both these two parameters are reduced.

Another variant of nanomesh, formed by periodic pattern of hydrogen clusters, has recently been observed for graphene grown on an iridium substrate.⁷ The periodicity is due to the fact that the composite structure of graphene and iridium forms a superlattice, with the hydrogenation occurring preferentially on specific superlattice sites. The resulting structure can be regarded as a variant of the nanomesh since regions of hydrogenated graphene are highly insulating.^{8–10} Nanomesh via patterned hydrogenation is a promising approach, since its cluster size and neck width can be much smaller than the lithographically defined case. Indeed, the opening of a substantial energy gap has been revealed by angle-resolved photoemission spectroscopy (ARPES).⁷

Theoretical investigations of the electronic properties of nanomesh/pattern-hydrogenated graphene have been limited so far to band-structure calculations using primitive supercells.^{5,7,11,12}

This approach can treat disorder in the cluster shape only within the same supercell.⁷ Instead, in this work, we present a modeling study of pattern-hydrogenated graphene that also includes disorder across different supercells. Through calculations of the momentum-energy-resolved density of states and its electrical conduction, we study the scaling of the energy gap on the parameters defining the patterned hydrogenation, i.e., cluster size, filling factor, and neck width.

The Model. A simple tight-binding (TB) model is employed to describe the composite structure of graphene with adsorbed hydrogen atoms.^{13,14} Within this model, the basis consists of a $2p_z$ orbital per carbon atom and a $1s$ orbital per hydrogen atom: the parameters describing the carbon–carbon hopping integral ($\gamma = 2.6$ eV), carbon–hydrogen hopping integral ($\gamma_{\text{H}} = 5.72$ eV), and hydrogen onsite energy ($\epsilon_{\text{H}} = 0$ eV) are taken from ref 14. Such a minimal model captures the essential physics of the hydrogenation effect pertinent for our study, that is, the removal of the p_z orbital of the hydrogenated carbon atom from the π and π^* bands.¹⁵ Since our purpose is to study the intrinsic properties of the nanomesh, we neglect the interaction with the iridium substrate in the TB model. As a consequence, particle–hole symmetry is preserved and the neutrality point remains located at the Dirac point.

Graphene on an iridium substrate forms a superlattice due to the mismatch between their respective lattice constants; 10×10 graphene unit cells are commensurate with 9×9 iridium unit cells.¹⁶ The superlattice unit cell is represented in Figure 1a. The supercell preserves the symmetry of the graphene unit cell,¹⁷ resulting in a honeycomb superlattice. Experimentally,⁷ it was

Received: May 22, 2011

Revised: October 10, 2011

Published: October 14, 2011

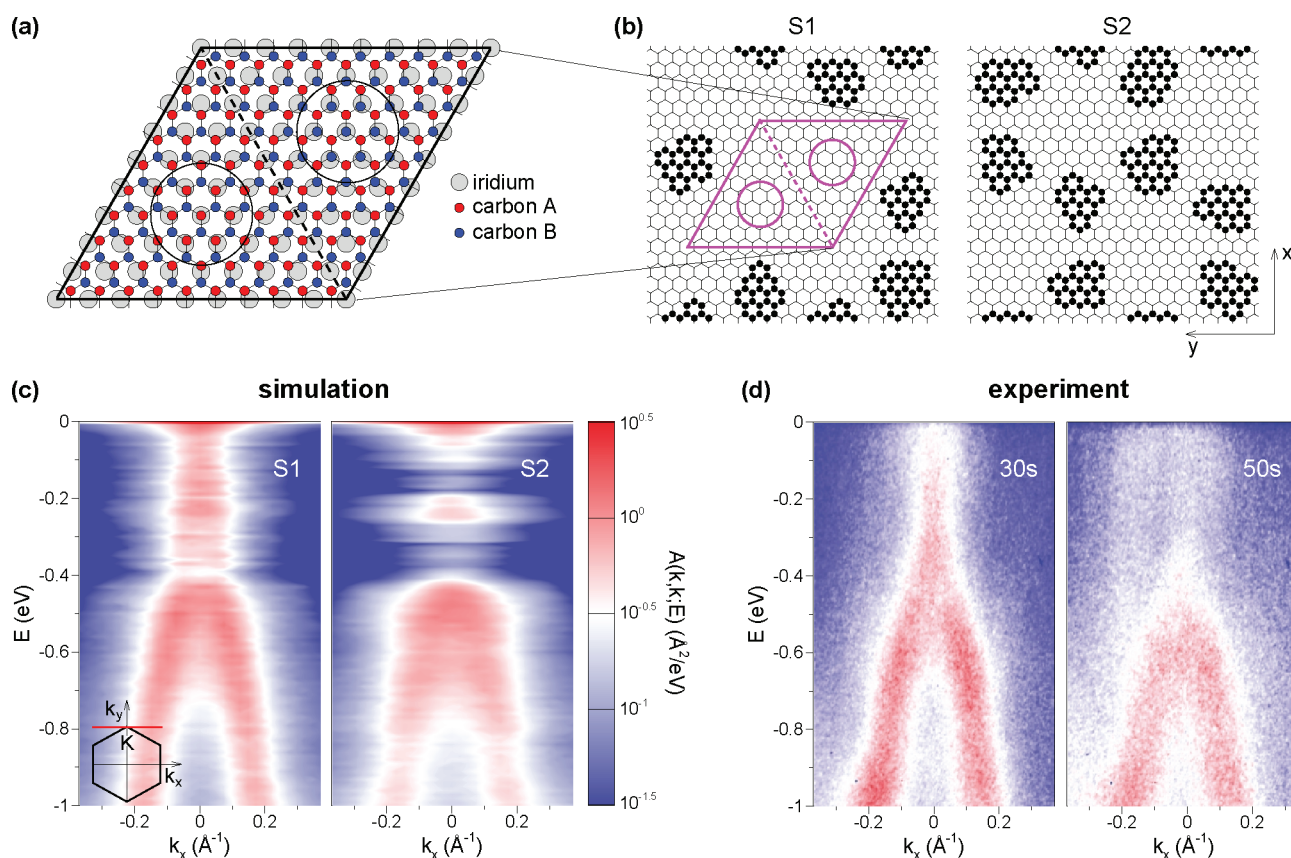


Figure 1. Schematic representation of the atomic structure under study and comparison of the simulated k -resolved density of states in energy with the experimental ARPES. (a) Top view of the supercell of graphene on iridium substrate. The two graphene sublattices are indicated with different colors. The supercell is symmetric under reflection across the dashed line, except for the interchange of the two graphene sublattices. The two circles highlight the regions of the supercell where the clusters tend to form. (b) Top view of two hydrogenated samples with different cluster concentration. Hydrogen atoms are represented as black dots on the honeycomb graphene lattice and the iridium substrate is not shown. S1 is obtained with the model parameters $N_w = 4$, $n_c = 0.75$, while S2 with $N_w = 4$, $n_c = 1$. (c) Calculated momentum-energy resolved density of states for two sets of hydrogenated samples that correspond to the cases S1 and S2 shown in (b). 50 samples are considered for each set, the plotted quantity being the average. The inset shows the direction within the graphene Brillouin zone (red line) along which the calculation is performed. (d) Experimental ARPES intensity for different times of exposure to hydrogen (as indicated in the labels). Reprinted with permission from ref 7. Copyright 2010 Macmillan Publishers Ltd.

shown that the hydrogen clusters tend to form in regions indicated by circles in Figure 1a, where one graphene sublattice sits directly on top of iridium atoms. A hydrogenation model is developed to reproduce this preferential adsorption (see details in the Supporting Information). The model takes as input two parameters: a discrete quantity N_w which represents the cluster radius, and the filling factor n_c , i.e., ratio between the number of clusters and the number of half-supercells. Two types of disorder are considered: (i) irregular cluster edges and (ii) a random filling of the superlattice (if $n_c < 1$). See Figure 1b for illustrations. Each cluster is generated by adding hydrogen atoms on top of the carbon atoms belonging to a certain number of shells around the center of the half-supercell, and the edge disorder is introduced by partial hydrogenation of the outer shell. Both A and B sites are hydrogenated within each cluster, contrary to what is expected in the real structure.⁷ The additional hydrogen atoms play the role of the neglected interactions with the substrate in removing the pseudodangling bonds.^{7,18}

Key Features in Momentum-Energy Resolved Density of States. In order to study the electronic properties of pattern-hydrogenated graphene as seen in ARPES experiments, calculation of the momentum-energy resolved density of states is required. This quantity is given, apart from a normalization

factor, by the diagonal elements of the spectral function in momentum space, $A(\mathbf{k}, \mathbf{k}; E)$. While this quantity reduces to the usual band structure for periodic systems, it is a general concept and is valid even for disordered systems. The calculation is performed by first computing the spectral function in real space $A(\mathbf{r}, \mathbf{r}'; E)$ and then Fourier transforming to get $A(\mathbf{k}, \mathbf{k}; E)$.¹⁹ The calculation is done using Green's function formalism with a recursive algorithm for periodic structures. See the Supporting Information for detailed numerical description and implementation.

In Figure 1c, we plot the averaged $A(\mathbf{k}, \mathbf{k}; E)$ for two ensembles corresponding to the two realizations shown in Figure 1b, along a path in k -space that includes the K point.²⁰ The convergence of the result with respect to sample size and ensemble size has been checked, as reported in the Supporting Information. Only the negative energies are shown, as the conduction bands are symmetrical to the valence ones due to particle–hole symmetry. The corresponding experimental ARPES image⁷ corresponding to two different hydrogen doses is shown in Figure 1d. Several distinctive features are observed in both simulations and experiments. In both cases, the two valence branches intersect at a lower energy than the Dirac point. In addition, the signal of the states lying at the K point between $E = 0$ and the intersection

energy gets suppressed with increasing hydrogen doping. These features can be interpreted as a band gap opening. The presence of a flat band at $E = 0$ in the simulation results is a well-known effect, due to the imbalance between the two graphene sublattices.²¹ The absence of these states in the experimental ARPES could be related to bond relaxation and sp^3 hybridization,²² which are neglected in the simulations.

Scaling of Energy Gap. The energy gap is extracted from the momentum-energy-resolved density of states for different sets of samples, corresponding to different values of cluster size, filling factor, and supercell size. The supercell size is increased by considering a fictitious substrate other than iridium: for fixed cluster size, this corresponds to increasing the neck width. Figure 2a illustrates the fitted band edges from $A(\mathbf{k}, \mathbf{k}; E)$, with details in the Supporting Information. An apparent universal scaling relation for the band gap is obtained when we plot the extracted band gap values E_g (together with a measure of the broadening of each $A(\mathbf{k}, \mathbf{k}; E)$ plot as error bar) against the quantity $N_H^{1/2}/N_C$, where N_H and N_C are the average number of hydrogen and carbon atoms in the half-supercell (Figure 2b).²³ A similar relation also applies for the case of triangular graphene nanomesh.⁵ In ref 11, it was stated that a universal relation does not hold for honeycomb graphene nanomesh. However, Figure 2b suggests that when disorder is included in the simulations, the scaling law $E_g = c(N_H^{1/2})/N_C$, with c a constant, can be valid at low defect coverage for honeycomb superlattices as well. This is similar to the case of graphene nanoribbons, where theoretically the band gap depends on the precise atomic configuration,²⁴ while a general law $E_g \propto 1/W$, with W the ribbon width, is always observed in the experiments³ and commonly attributed to disorder.^{25,26} Regarding the proportionality constant, we found that the expression $c = 2\hbar v_F \pi / (A_s/2)^{1/2}$, with v_F the graphene Fermi velocity and A_s the area of the graphene unit cell, fits fairly well the numerical data (dashed line in Figure 2b). We note that by defining $\Delta = (A_s/2)^{1/2} (N_C/N_H^{1/2})$, the scaling relation takes the form $E_g = 2\hbar v_F \pi / \Delta$. This equation can be thought of as arising from the quantization of the graphene dispersion relation $E = \pm \hbar v_F |\mathbf{k}|$ (\mathbf{k} is here the wave vector around the K point) with $|\mathbf{k}| = \pi / \Delta$ (1D quantization in random directions): Δ can thus be interpreted as an effective confinement length.

Transport Gap. Next, we examine the electronic transport properties of pattern-hydrogenated graphene. Techniques for the transfer of graphene grown on metal surfaces to an insulating substrate have recently been developed.²⁸ We consider a three-terminal structure as shown in Figure 3a and aim at predicting its low-temperature, low-bias conductance. Figure 3b illustrates the potential energy along the device. The potential energy in the source and drain leads, as a result of metal induced doping, is kept fixed with respect to the Fermi level E_F . The channel potential V_{ch} is modulated by the back gate. Graphene is aligned with its armchair direction along the longitudinal direction of the device, in order to avoid edge transport effects. Only the channel is hydrogenated while the leads are pristine graphene. The conductance is computed by using the standard Green's function technique²⁹ combined with a modified version of the algorithm described in ref 30, which is commonly used for the calculation of the lead self-energies (see Supporting Information).

Figure 3c shows the simulated, ensemble averaged zero-temperature conductance G vs V_{ch} . The device size is kept fixed at $W = L = 30$ nm, while different sets of hydrogenated samples are considered. It can be seen that patterned hydrogenation leads to a clear transport gap, increasing with N_w and n_c . Also, the

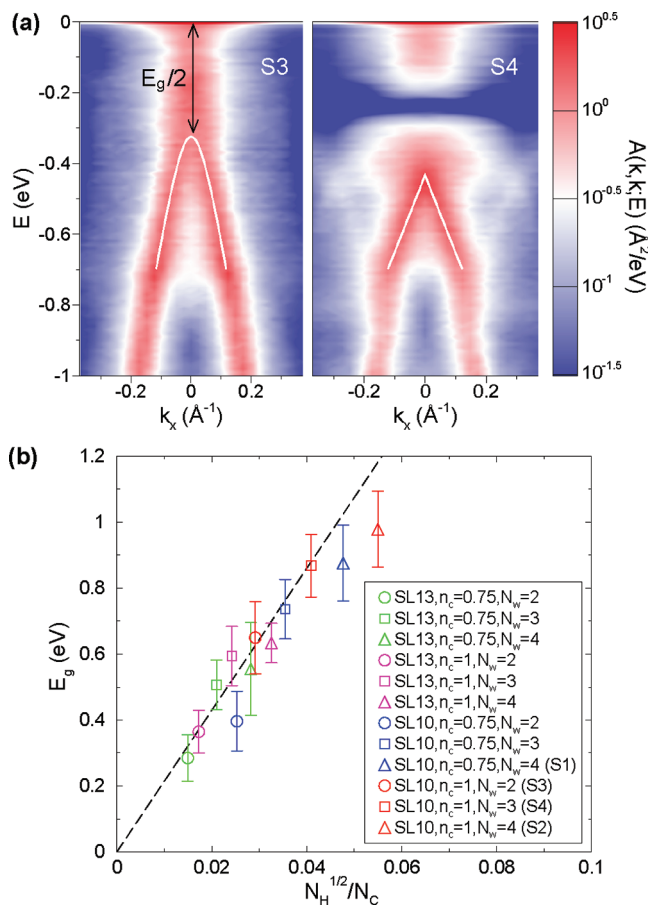


Figure 2. Band-gap extraction. (a) Momentum-energy resolved density of states for two sets of hydrogenated samples on iridium substrate: S3 is obtained with the model parameters $N_w = 2$, $n_c = 1$, while S4 with $N_w = 3$, $n_c = 1$. Different fitting curves are used (white lines), given by eqs 31 and 29 in the Supporting Information, for S3 and S4, respectively. The band gap is extracted with respect to the fitting curve. (b) Band gap extracted for the various sets of samples and plotted as a function of $N_H^{1/2}/N_C$, where N_H and N_C are the average number of hydrogen and carbon atoms in the half-supercell, respectively. The fitting functions used for the extraction are listed, for each set, in Table 1 of the Supporting Information. SL10 stands for graphene on iridium substrate (supercell made of 10×10 graphene unit cells, see Figure 1a), while SL13 refers to graphene on a fictitious substrate (supercell made of 13×13 graphene unit cells). The error bar is a measure of the broadening of the $A(\mathbf{k}, \mathbf{k}; E)$ plot. The dashed line is the curve $E_g = 2\hbar v_F \pi / \Delta$, with $v_F = (3/2)a_{CC}|\gamma|/\hbar$ the Fermi velocity in pristine graphene and $\Delta = (A_s/2)^{1/2} (N_C/N_H^{1/2})$, where a_{CC} is the carbon-carbon distance and $A_s = a_{CC}^2 3(3^{1/2})/2$ the area of the unit cell of pristine graphene.

transport simulations agree well with our band-structure results: the transport gap matches the band gap from the $A(\mathbf{k}, \mathbf{k}; E)$ fitting (as indicated by vertical lines in Figure 3c) and the peaks in the transport gap region correspond to the gap states in $A(\mathbf{k}, \mathbf{k}; E)$.³¹ The G vs V_{ch} curve appears symmetrical, unlike the case for pristine graphene.³² This suggests that scattering is dominated by the channel, instead of the tunneling resistance due to pn junctions.

Scaling of Transport Coefficients. Finally, we examine how G scales with L . Here, we consider devices with filling factor $n_c = 1$. The conductance is found to scale as $G \propto \exp(-L/\xi)$, where ξ is a decay length. Figure 4a plots the extracted ξ as a function of V_{ch} bias, while Figure 4b illustrates the extraction of ξ for two

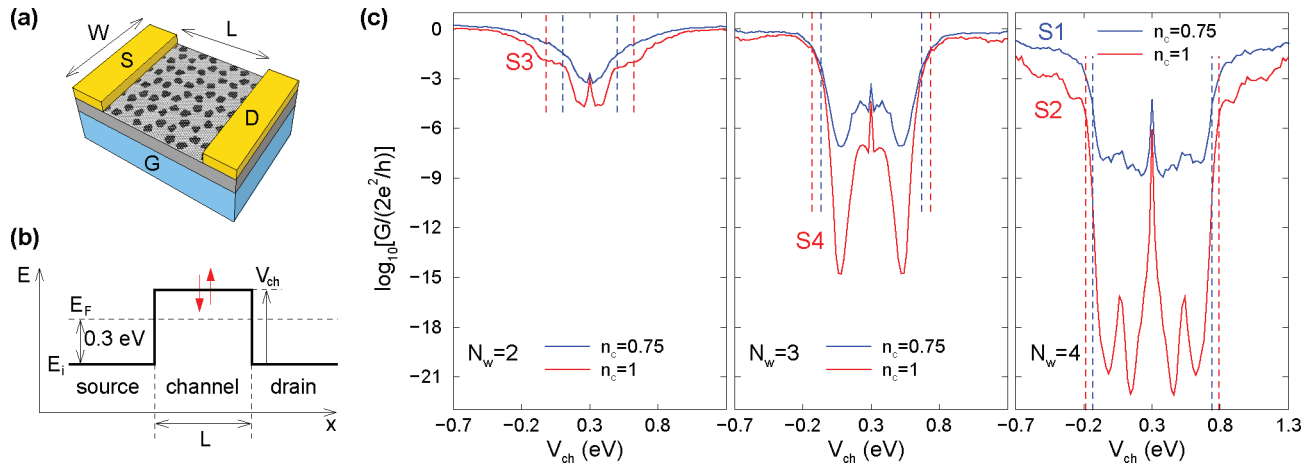


Figure 3. Transport simulations. (a) Conceptual device under investigation: pattern-hydrogenated graphene is transferred to an insulating substrate and used as channel material of a field-effect transistor. (b) Profile of the potential energy used to simulate the structure in (a): the Fermi level in the leads E_F is kept fixed, while the barrier height V_{ch} is varied to reproduce the effect of the back gate. Pristine graphene is used for the leads. (c) Zero-temperature conductance vs V_{ch} for various sets of samples with $W = L = 30$ nm and iridium substrate (SL10). From left to right, the cluster size, i.e., N_w , is increased; within the same plot, the cluster concentration n_c is varied. 100 samples are considered for each set, and the average is done on the logarithm of the normalized conductance (a motivation for this type of averaging can be found in ref 27). The vertical lines indicate the band gap from Figure 2b.

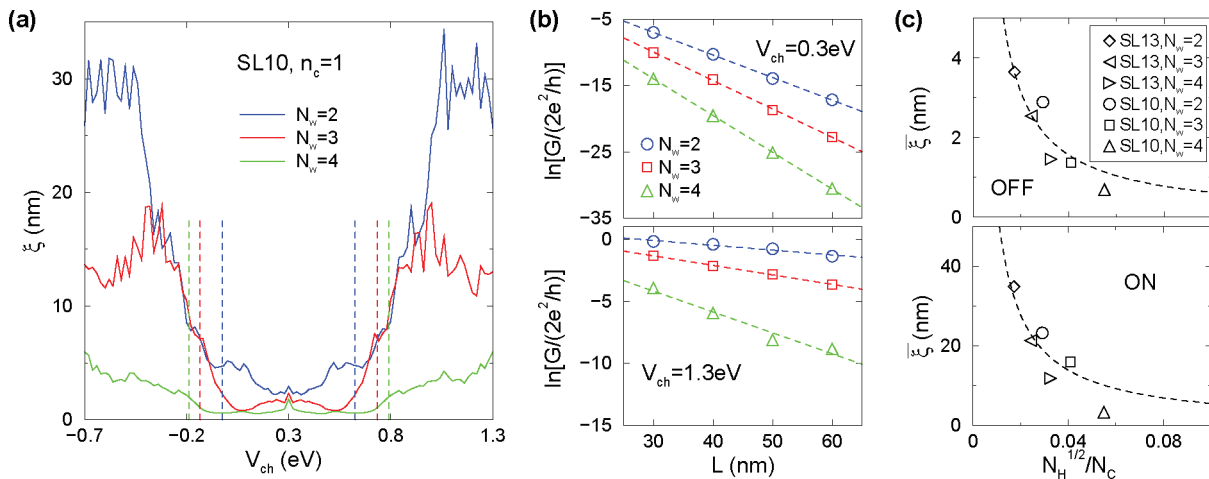


Figure 4. Decay length extraction. (a) Decay length vs V_{ch} for sets of samples with different cluster size and fixed supercell size (SL10) and cluster concentration ($n_c = 1$). The vertical lines indicate the band gap from Figure 2b. (b) Example of the decay length extraction at two different V_{ch} points. The dashed lines indicate the fitting with the formula $\ln[G/(2e^2/h)] = \ln g_0 - L/\xi$. (c) Average value of the decay length in the “off” and “on” state for various sets of samples with different supercell and cluster sizes, plotted as a function of $N_H^{1/2}/N_C$. The dashed lines indicate the fitting curve $\bar{\xi} \propto N_C/N_H^{1/2}$. The off state is defined as the bias region $|V_{ch} - E_F| < E_G/2 - B$, where B is the half-broadening from Figure 2b, while the on state is defined as $0.65 \text{ eV} < |V_{ch} - E_F| < 0.75 \text{ eV}$.

particular V_{ch} values. Next, we extract the average value $\bar{\xi}$ of the decay length in the “off” and “on” state and plot it against $(N_H)^{1/2}/N_C$ as we have done previously for the band gap (Figure 4c, see caption for the definition of the “on” and “off” states). One observes that, for almost all the samples, the value of the decay length in the “off” state is about an order of magnitude smaller than the corresponding value in the “on” state. For both cases, the average decay length seems to follow the general scaling law $\bar{\xi} \propto N_C/N_H^{1/2}$ at low to moderate hydrogenation concentrations, albeit the “off” state exhibits a smaller proportionality constant. We note that in the “off” state the exponential decrease of G with L can be explained as evanescent transport through a clean band gap;²⁵ the scaling law $\bar{\xi} \propto \Delta \propto 1/E_g$ is in agreement with this interpretation. In the “on” state instead, the exponential decrease

of G with L is an effect of quantum localization due to disorder and ξ takes the meaning of a localization length.³³ The scaling law $\bar{\xi} \propto \Delta$ is here less clear and an exponential dependence could also be possible, as suggested by recent experiments.³⁴ Moreover, dephasing effects, which are ignored in our simulations, could restore a diffusive transport regime, $G \propto 1/L$, as the temperature is raised.

Conclusions. In conclusion, a simple model for pattern-hydrogenated graphene was presented. Similar features are observed in the calculated k -resolved density of states in energy and in the experimental ARPES. The scaling of the energy gap on the parameters N_C and N_H was presented, including its electronic transport properties at low temperature. Our results indicate that pattern-hydrogenated graphene is a promising approach to the

engineering of graphene nanomeshes with extremely scaled cluster sizes and neck widths.

■ ASSOCIATED CONTENT

S **Supporting Information.** Details on the hydrogenation model, procedure for the band gap extraction, and numerical algorithms. This material is available free of charge via the Internet at <http://pubs.acs.org>.

■ AUTHOR INFORMATION

Corresponding Author

*E-mail: rgrassi@arces.unibo.it.

Present Addresses

^SIBM T.J. Watson Research Center, Yorktown Heights, NY 10598, USA.

■ ACKNOWLEDGMENT

The authors gratefully acknowledge support from Network for Computational Nanotechnology for computational services.

■ REFERENCES

- Geim, A. K.; Novoselov, K. S. *Nat. Mater.* **2007**, *6*, 183.
- Neto, A. H. C.; Guinea, F.; Peres, N. M. R.; Novoselov, K. S.; Geim, A. K. *Rev. Mod. Phys.* **2009**, *81*, 109.
- Han, M. Y.; Özyilmaz, B.; Zhang, Y.; Kim, P. *Phys. Rev. Lett.* **2007**, *98*, 206805.
- Wang, X.; Ouyang, Y.; Li, X.; Wang, H.; Guo, J.; Dai, H. *Phys. Rev. Lett.* **2008**, *100*, 206803.
- Pedersen, T. G.; Flindt, C.; Pedersen, J.; Mortensen, N. A.; Jauho, A.-P.; Pedersen, K. *Phys. Rev. Lett.* **2008**, *100*, 136804.
- Bai, J.; Zhong, X.; Jiang, S.; Huang, Y.; Duan, X. *Nat. Nanotechnol.* **2010**, *5*, 190.
- Balog, R.; Jørgensen, B.; Nilsson, L.; Andersen, M.; Rienks, E.; Bianchi, M.; Fanetti, M.; Laegsgaard, E.; Baraldi, A.; Lizzit, S.; Slijivancanin, Z.; Besenbacher, F.; Hammer, B.; Pedersen, T. G.; Hofmann, P.; Horneker, L. *Nat. Mater.* **2010**, *9*, 315.
- Sofo, J. O.; Chaudhari, A. S.; Barber, G. D. *Phys. Rev. B* **2007**, *75*, 153401.
- Elias, D. C.; Nair, R. R.; Mohiuddin, T. M. G.; Morozov, S. V.; Blake, P.; Halsall, M. P.; Ferrari, A. C.; Boukhvalov, D. W.; Katsnelson, M. I.; Geim, A. K.; Novoselov, K. S. *Science* **2009**, *323*, 610.
- Fiori, G.; Lebègue, S.; Betti, A.; Michetti, P.; Klinton-berg, M.; Eriksson, O.; Iannaccone, G. *Phys. Rev. B* **2010**, *82*, 153404.
- Petersen, R.; Pedersen, T. G.; Jauho, A.-P. *ACS Nano* **2011**, *5*, 523.
- Yang, M.; Nurbawono, A.; Zhang, C.; Feng, Y. P.; Ariando *Appl. Phys. Lett.* **2010**, *96*, 193115.
- Robinson, J. P.; Schomerus, H.; Oroszlány, L.; Fal'ko, V. I. *Phys. Rev. Lett.* **2008**, *101*, 196803.
- Bang, J.; Chang, K. J. *Phys. Rev. B* **2010**, *81*, 193412.
- As explained in ref 13, the effect of each hydrogen atom at energy E can be recast in a effective self-energy $\Sigma_H = \gamma_H^2 / (E + i0^+ - \epsilon_H)$ for the attached carbon orbital: since $\Sigma_H \gg 1$ eV for $0 < |E| < 1$ eV, the hydrogenated carbon atom effectively acts as a vacancy in the energy range of interest.
- N'Diaye, A. T.; Bleikamp, S.; Feibelman, P. J.; Michely, T. *Phys. Rev. Lett.* **2006**, *97*, 215501.
- It can be divided into two regions that are equivalent to each other under reflection, apart from the exchange of the two graphene sublattices.
- Brako, R.; Šokčević, D.; Lazić, P.; Atodiresei, N. *New J. Phys.* **2010**, *12*, 113016.
- More precisely, within the TB representation, the continuous position \mathbf{r} is substituted by the pair $(\mathbf{l}; q)$, with \mathbf{l} the graphene lattice vector and q the orbital index: the projected spectral function for carbon atoms only is considered ($q = 1, 2$), the Fourier transform is done with respect to \mathbf{l} , and the result is summed over q , that is over the two graphene sublattices (an additional factor is used in our plots to normalize the number of states with respect to the graphene unit cell; spin degeneracy is not included).
- We note the absence of repeating dispersions expected for a periodic superlattice structure. This is due to the effect of disorder, which destroys the strict periodicity.
- Pereira, V. M.; dos Santos, J. M. B. L.; Neto, A. H. C. *Phys. Rev. B* **2008**, *77*, 115109.
- Boukhvalov, D. W.; Katsnelson, M. I.; Lichtenstein, A. I. *Phys. Rev. B* **2008**, *77*, 035427.
- For constant supercell size and filling factor, the points seem to depart from the linear trend. This could be explained by the fact that, for some ensembles, the amount of disorder on the cluster edges is not strong enough to completely wash out the interference effect of the specific cluster shape. This situation is particularly evident for $N_w = 3$, where the repeated band structure of the superlattice is still distinguishable in the $A(\mathbf{k}, \mathbf{k}; E)$ plot (see Figure 2a-right and additional plots in the Supporting Information).
- Son, Y.-W.; Cohen, M. L.; Louie, S. G. *Phys. Rev. Lett.* **2006**, *97*, 216803.
- Gunlycke, D.; Areshkin, D. A.; White, C. T. *Appl. Phys. Lett.* **2007**, *90*, 142104.
- Han, M. Y.; Brant, J. C.; Kim, P. *Phys. Rev. Lett.* **2010**, *104*, 056801.
- Anderson, P. W.; Thouless, D. J.; Abrahams, E.; Fisher, D. S. *Phys. Rev. B* **1980**, *22*, 3519.
- Li, X.; Cai, W.; An, J.; Kim, S.; Nah, J.; Yang, D.; Piner, R.; Velamakanni, A.; Jung, I.; Tutuc, E.; Banerjee, S. K.; Colombo, L.; Ruoff, R. S. *Science* **2009**, *324*, 1312.
- Datta, S. *Electronic Transport in Mesoscopic Systems*; Cambridge University Press: Cambridge and New York, 1997.
- Sancho, M. P. L.; Sancho, J. M. L.; Rubio, J. *J. Phys. F: Met. Phys.* **1985**, *15*, 851.
- We note that, since the transport simulations confirm the previously extracted gap size, the gap is expected to have the same extension in other directions than the one used for Figures 1c and 2a.
- Low, T.; Hong, S.; Appenzeller, J.; Datta, S.; Lundstrom, M. S. *IEEE Trans. Electron Devices* **2009**, *56*, 1292.
- Lee, P. A.; Ramakrishnan, T. V. *Rev. Mod. Phys.* **1985**, *57*, 287.
- Jaiswal, M.; Lim, C. H. Y. X.; Bao, Q.; Toh, C. T.; Loh, K. P.; Özyilmaz, B. *ACS Nano* **2011**, *5*, 888.